RESEARCH ARTICLE

Determining the origin and fate of nitrate in the Nanyang Basin, Central China, using environmental isotopes and the Bayesian mixing model

Shengwei Cao [1,2] · Yuhong Fei [1,2] · Xia Tian [1,2] · Xiangxiang Cui [1,2] · Xueqing Zhang [1,2] · Ruoxi Yuan [1,2] · Yasong Li [1,2]

Abstract
Identifying sources of nitrate contamination has been a long-term challenge in areas with different land uses. We investigated the biogeochemical processes and quantified the contribution of potential nitrate sources in the Nanyang Basin, the source area of the South to North Water Diversion Project in China. Hydrogeochemical characteristics, the dual-isotope method (δ^{15}N-NO$_3^-$ and δ^{18}O-NO$_3^-$), and the Bayesian mixing model (SIAR) were combined. The results for 160 samples indicated that mean nitrate concentrations of residential area (162.83 mg L^{-1}) and farmland (75.71 mg L^{-1}) were higher compared with those of surface water (16.15 mg L^{-1}) and forest (36.25 mg L^{-1}). Hydrochemical facies and molar ratios of major ions indicated that the natural environment was greatly impacted by anthropogenic activities. Nitrification, ammonium volatilization, and mixing effects were the dominant processes in nitrogen transformation. The contributions of different sources to nitrate contamination were 45.41%, 35.81%, 17.87%, and 0.91% for sewage and manure, soil organic nitrogen, synthetic fertilizer, and atmospheric deposition, respectively. Undeveloped infrastructure and sewage disposal in rural areas were the main causes of nitrate contamination. Our results provide a theoretical basis for the development of measures to guarantee long-term water supply of the South to North Water Diversion Project.

Keywords Nitrate contamination · South to North Water Diversion Project · Stable isotope · Groundwater

Highlights
1. We investigated the impacts of diverse land uses and anthropogenic activities on nitrate in groundwater.
2. Dual-isotope composition illustrated that sewage and manure were the main pollution source.
3. Nitrification and ammonium volatilization were the dominant factors causing variations in isotopic composition.
4. Limitations of the dual-isotope method mask the potential sources of nitrate contamination.

Responsible Editor: Philippe Garrigues

✉ Yasong Li
  liyasong@mail.cgs.gov.cn

  Shengwei Cao
  caoshengwei_hei@163.com

  Yuhong Fei
  yuhong_fei@163.com

  Xia Tian
  tianxia429@126.com

  Xiangxiang Cui
  cuixiang2008@126.com

  Xueqing Zhang
  364471331@qq.com

  Ruoxi Yuan
  234408031@qq.com

[1] Institute of Hydrogeology and Environmental Geology, Chinese Academy of Geological Sciences, No.256, North Zhonghua Street, Xinhua District, Shijiazhuang, Hebei Province, China

[2] Hebei Province and China Geological Survey, Key Laboratory of Groundwater Remediation, No.256, North Zhonghua Street, Xinhua District, Shijiazhuang, Hebei Province, China

🖄 Springer

Introduction

Groundwater represents the largest store of unfrozen freshwater on earth (Aeschbach and Gleeson 2012). Influenced by increasingly intensive anthropogenic activities, such as inadequate fertilizer application or inefficient sewage disposal, many groundwater basins show increased levels of nitrate (Chaudhuri et al. 2012; Kaushal et al. 2011; Wang et al. 2017), resulting in water quality degradation (Elisante and Muzuka 2015; Rahmati and Melesse 2016). In addition, water eutrophication may occur, as well as negative impacts on human health (Camacho-Cruz et al. 2020; Wu et al. 2018), such as the "blue baby syndrome" and stomach cancer (Dan-Hassan et al. 2012; Knobeloch et al. 2000). Generally, NO_3^- concentrations above 13.39 mg L^{-1} indicate groundwater contamination as a result of human activities (Burkart and Kolpin 1993). The World Health Organization has established a nitrate value of 50 mg L^{-1} as the maximum allowed concentration (MAC) for drinking water (WHO 2003).

Nitrate, as the end product of nitrification process, is less bioavailable in soils (Lunau et al. 2012), and hence, nitrate contamination usually starts as a non-point source (Kaushal et al. 2011). Potential sources of nitrate are atmospheric deposition, soil N, manure, synthetic fertilizers, and wastewater from leaking sewerage networks or septic systems (Wang et al. 2017). Due to the complex transformation processes of nitrogen in aquifers, the most suitable approach to control nitrate contamination is identifying the potential sources and reducing the inputs (Ma et al. 2016; Wick et al. 2011). One method, the dual-isotope method (DIM, using $\delta^{15}N$–NO_3^- and $\delta^{18}O$–NO_3^-), can be used to assess which sources are predominantly responsible for nitrate contamination in an aquatic environment (Deutsch et al. 2006) and has been successfully applied in recent years (Kim et al. 2015; Wang et al. 2017; Zhang et al. 2018a, 2018b). However, in complex environments with multiple nitrogen (N) sources, this method is limited (Clagnan et al. 2017; Minet et al. 2017). Although different N sources involved in terrestrial N cycling have characteristic and recognizable isotope compositions in water samples (Kendall et al. 2008), the origin of nitrate must be linked to the entire N cycle, since isotope composition of nitrate can be biased due to different nitrate sources and kinetic isotopic fractionation (Li et al. 2019; Soto et al. 2019). These processes include assimilation during photosynthesis, mineralization, nitrification processes, and microbial denitrification in anoxic environments. For example, in the early stage of nitrification in non-N-limited systems (e.g., a fertilized field), the newly formed NO_3^- can be ^{15}N-depleted compared with the ammonia substrate due to the ^{15}N enrichment factor $\varepsilon NO_3^- - \varepsilon NH_4^+$, which ranges between −38 and −5‰ (Kendall et al. 2007). Also, nitrate assimilation during photosynthesis can cause large changes in the 1:1 relationship between the $\delta^{15}N$ and $\delta^{18}O$ of nitrate (Arce et al. 2014). As opposed to nitrification, denitrification mainly occurs in anaerobic environments, such as the hyporheic zone in rivers, with sufficient organic carbon and low oxygen concentrations (Huizenga et al. 2017). Isotopic enrichment caused by denitrification can cause an elevation of both $\delta^{15}N$–NO_3^- and $\delta^{18}O$–NO_3^-, resulting in an $\delta^{15}N$–NO_3^-:$\delta^{18}O$–NO_3^- ratio of the residual nitrate along a slope of approximately 1:2. In addition, volatilization results in the enrichment of $\delta^{15}N$–NO_3^- when nitrate is derived from manure and sewage (Spalding et al. 2018a, 2018b

Different sources may have an overlapping range of $\delta^{15}N$–NO_3^- and $\delta^{18}O$–NO_3^-, thus complicating the investigation of the causes of nitrate contamination. In such cases, calculation models such as IsoSource and SIAR have been used to quantify the contribution of different sources (Deutsch et al. 2006; Xue et al. 2009; Xue et al. 2012). The IsoSource program is based on the linear mixing model, which does not take the great uncertainty of N transformation process into consideration, such as the isotope fraction caused by nitrification, denitrification, and volatilization. The model uses the average isotope values from different sources, thereby ignoring the broad range of possible values of different sources (Liu et al. 2014). In this context, Xue (Xue et al. 2012) implemented a Bayesian isotope mixing model (SIAR) to determine the proportional contribution of different nitrate sources to six different surface waters. This program was developed based on the R language and can take more than three potential sources into consideration, regardless of the restrictions set by linear mixing model; it can calculate uncertainties at the same time and has therefore widely been used in recent years (Ding et al. 2015; Gautam and Iqbal 2010; Matiatos 2016; Meghdadi and Javar 2018a; Torres-Martínez et al. 2021). According to previous studies, there is no significant relationship between $\delta^{15}N$–NO_3^- or $\delta^{18}O$–NO_3^- vs. the NO_3^- concentration, suggesting that more than one biological process is responsible for the shifting of isotopic values (Archana et al. 2018). Therefore, additional indicators, such as major ions (e.g., SO_4^{2-}, Cl^-, NO_3^-, Br^-) and ionic ratios (e.g., Cl^-/Br^-, SO_4^{2-}/Cl^-, and Cl^-/NO_3^-), must be considered to better determine nitrate sources and transport processes (Murgulet and Tick 2013; Wang et al. 2013; Pasten-Zapata et al. 2014). As an addition factor, land use patterns play an important role in determining groundwater contamination (Taufiq et al. 2019), and the alteration of such patterns may have a direct impact on soil degradation (Sheikhy et al. 2017).

Geo-environmental surveys in the framework of the China Geology Survey (CGS) have revealed a deterioration trend in the environment of the shallow aquifer in the Nanyang Basin. In this area, groundwater quality of local aquifers directly affects water supply security of the South to North Water Diversion Project (SNWDP). However, studies investigating the N sources in this area are scarce (ChenMin-hua et al. 2011; Shi et al. 2012).

In this context, we focus on nitrate contamination of the Nanyang Basin, taking into account land use pattern analysis, the dual-isotope method (DIM), major ion analysis, and the Bayesian mixing model. The objectives of this study are as follows: (1) to determine the characteristics and distribution of nitrate contamination in the Nanyang Basin, (2) to combine DIM and hydrogeochemical characteristics of the shallow groundwater in the Nanyang Basin to identify the main processes controlling nitrate evolution, and (3) to perform source apportionment of nitrate contamination using SIAR. We provide a scientific basis for water quality management, with the aim to ensure the long-term water supply of the SNWDP.

Material and methods

Study area

The study area is located in the Nanyang Basin, Henan Province, in the most densely populated area in China. It covers an area of 18,242 km^2 (latitude between 31°50′ 33″ N and 33°20′ 25″ N, longitude between 111° 36′ E and 113° 34′ 45″) and is an important granary area in China. The origin of the middle route of the SNWDP, Danjiangkou Reservoir, is located on its middle western side (Fig. 1). Apart from the southern outlet, Nanyang Basin is enclosed by mountains on three sides. Dozens of medium-small creeks flow out of the valleys, constituting the river net in the basin and finally converging to local main rivers in the southern central plain of the Nanyang Basin. The area has a subhumid climate with an annual precipitation of 826.7 mm and an annual mean evaporation of 1449.2 mm (ChenMin-hua et al. 2011), and the annual mean temperature of study area is 16.8 °C (Du et al. 2017). Anthropogenic activities, such as agriculture and livestock breeding, have intensified in recent years.

Neotectonic movement since the early Pleistocene has largely been determining the landform and sedimental environment of the Nanyang Basin, thus controlling the characteristics of the main aquifers (Deng et al. 1996). The main aquifers of the basin can be divided into two groups: the upper aquifer (shallow aquifer) is unconfined or semi-confined, composed of Quaternary strata from the middle Pleistocene to the Holocene, lies at a depth of 10 to 50 m, and mainly consists of silty sand to coarser gravel. The second group is a confined aquifer at a depth of less than 200 m, composed of Neogene and early Pleistocene sediments. There is an aquitard between the two groups, mainly consisting of clay and silt, which impedes contaminant leaching to some extent. The shallow aquifer of the Nanyang Basin is mainly recharged by precipitation and the lateral flow from piedmont areas surrounding the basin and is the primary water source in Nanyang Basin. In recent years, due to the increasing water demand, both surface water and groundwater level continue to decline, and the interaction between surface and groundwater becomes more complicated especially during dry season. The southern outlet of the basin and the main channel of local water, going north–south through the center of the study area, are sinks for both groundwater and surface water (Fig. 1). Most of the groundwater supply is pumped from the alluvial deposit, which is rich in gravel and coarse sands, in the first and second terraces along both sides of the plain.

China is the world's greatest producer and user of fertilizers, applying about 31% of the total amount of fertilizers used worldwide (FAO 2020; Su et al. 2013). Agricultural fertilization is common in the study area, which may result in severe nitrate contamination of the local rivers and aquifers (Ju et al. 2006; Wang et al. 2015; Piske and Peterson 2020). In the last 10 years, chemical fertilizers, such as urea and a NPK compound fertilizer, have typically been applied at rates of approximately 750–850 kg ha^{-1} year^{-1} for winter wheat and summer maize, whereas in the 1980s, rates were only about 200 kg ha^{-1} year^{-1}. Although the Nanyang Basin is densely populated, its infrastructure is relatively undeveloped, and a part of the sewage is directly discharged into sinkholes or rivers, aggravating nitrate contamination of the groundwater.

Since land use patterns can have an impact on non-point source pollution, we analyze land use types via ENVI 5.3, using remote sensing image data for 2015 (Landsat OLI_TIRS8) (Fig. 2). The areas of different land use types in the study area are summarized in Supplemental Material (Table S2). Based on remote sensing analysis, the land use types in the study area were farmland (79.84% of total study area), residential area (12.82%), forest (4.1%), and surface water (2.77%). The area of other types such as grass land and bare land is negligible.

Field survey, sampling, and analysis

Filed survey and sampling

Field survey and sample collection were conducted in November 2016 for the entire basin and in June 2017 for a typical nitrate-contaminated area in the Nanyang Basin (see "Stable isotope composition of nitrate" for details). At each sampling point, depth to groundwater, electrical conductivity (EC), pH, dissolved oxygen (DO), and oxidation–reduction potential (ORP) were measured in situ (HQD 30, Hach, USA); groundwater depth was measured using a water level meter (model 102, Solinst, USA). In total, 160 water samples were collected, including surface water, shallow aquifer water, and deep aquifer water. Figure 1 shows the location of each sample and its nitrate concentration. Except for NO$_3^-$, the major ions in water (Na$^+$, K$^+$, Ca^{2+}, Mg^{2+}, NO$_2^-$, NH$_4^+$, SO$_4^{2-}$, HCO$_3^-$, CO$_3^{2-}$, Fe, and Mn) were analyzed for each sample. Water samples were collected in 500-mL acid-
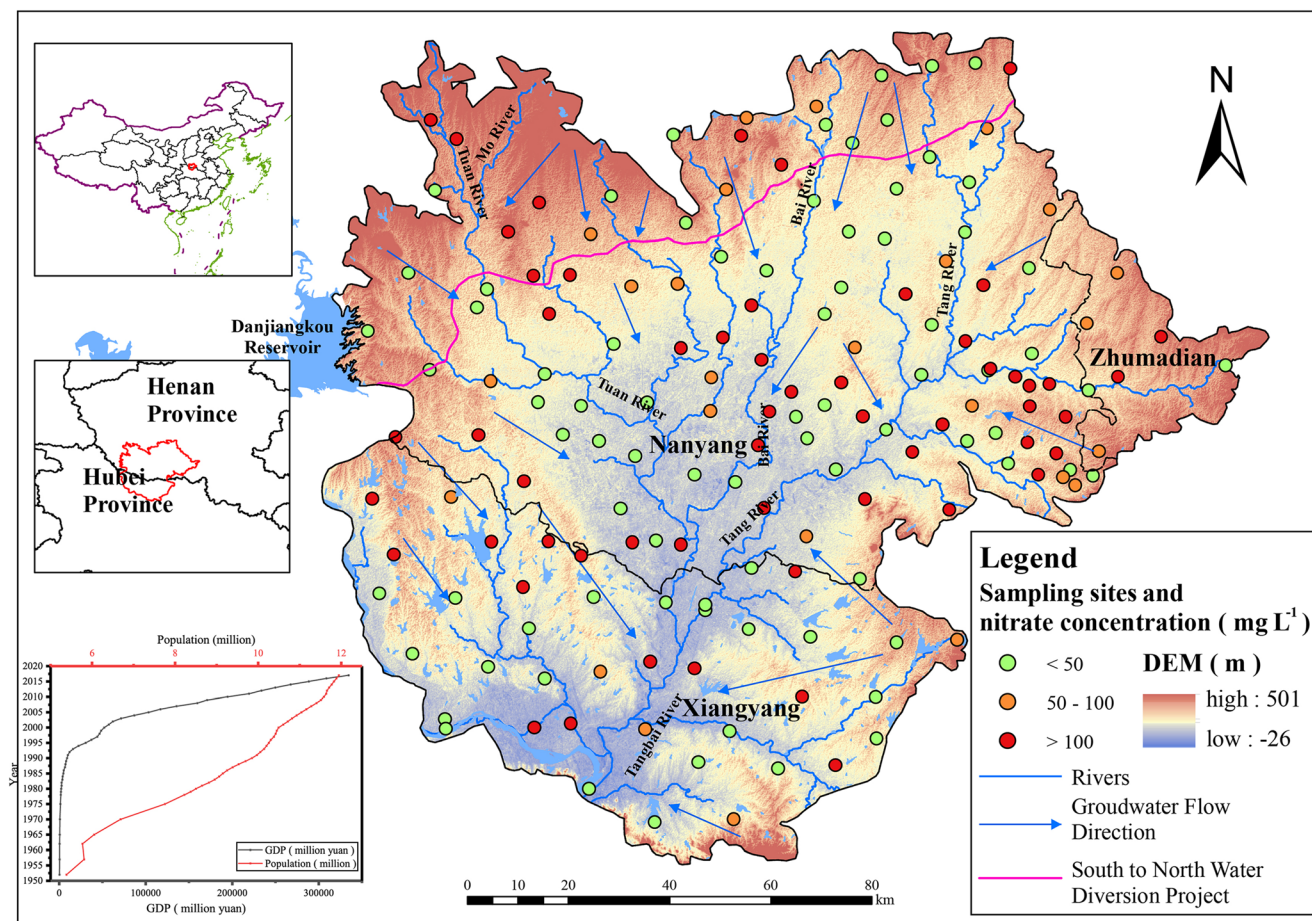
Fig. 1 Location of the Nanyang Basin in China (upper left), relation between population and GDP since 1952 (lower left), DEM, nitrate sample location, and nitrate concentration levels (center). Statistical data were obtained from the Nanyang Statistical Yearbook; the concentrations of nitrate are based on the groundwater quality standard of China

washed polyethylene bottles, using a high-density polyethylene sampler, filtered through 0.45 μm membranes, transported to the laboratory, and stored at 4 °C prior to analysis (maximum storage time: 1 week).

A typical nitrate-contaminated area was selected based on data from the analysis at the whole-basin scale ($n = 28$). For these 28 samples, according to judgement getting from the inquiries to residents during field survey that whether the sampling sites are potentially threatened by nitrate contamination, 12 of them were selected to analysis the ratios of stable isotopic N and O of NO_3^-, as well as the composition of δD-H_2O and $\delta^{18}O$-H_2O (5 samples).

Sample analysis

In the laboratory, the concentrations of anions (Cl^-, SO_4^{2-}, NO_3^-, NO_2^-) were measured by spectrophotometry (Perkin-Elmer Lambda 35, USA) with a precision of 5%. The analysis of cations (Na^+, K^+, Ca^{2+}, Mg^{2+}, Fe, Mn) in the water samples was performed via inductively coupled plasma-mass spectrometry (Agilent 7500ce ICP-MS, Tokyo, Japan). NH_4^+

was analyzed by Nessler's reagent spectrophotometric methods with a precision of ± 2%. Total alkalinity (as HCO_3^-) was determined by titration with standard 0.1 N hydrochloric acid, using methyl orange and phenolphthalein as indicators, with a precision of ± 5%. All major ion results were accepted only when the charge balance error was within ± 6.5%, and many were better than ± 3% (Table S1 in Supplemental Material). These measurements were performed at the Groundwater Mineral Water and Environmental Monitoring Center at the Institute of Hydrogeology and Environmental Geology, Chinese Academy of Geological Sciences.

The values of δ^2H-H_2O and $\delta^{18}O$-H_2O were analyzed by the Key Laboratory of Groundwater Sciences and Engineering, Ministry of Natural Resources, China. The $\delta^{18}O$ value was determined using CO_2–H_2O equilibration mass spectrometry, and the δD value was determined using H_2–H_2O equilibration-mass spectrometry under the catalysis of platinum, followed by analysis with a MAT253 gas isotope mass spectrometer. The isotope results were reported as relative (per mil) deviation from the isotopic ratio of the sample,
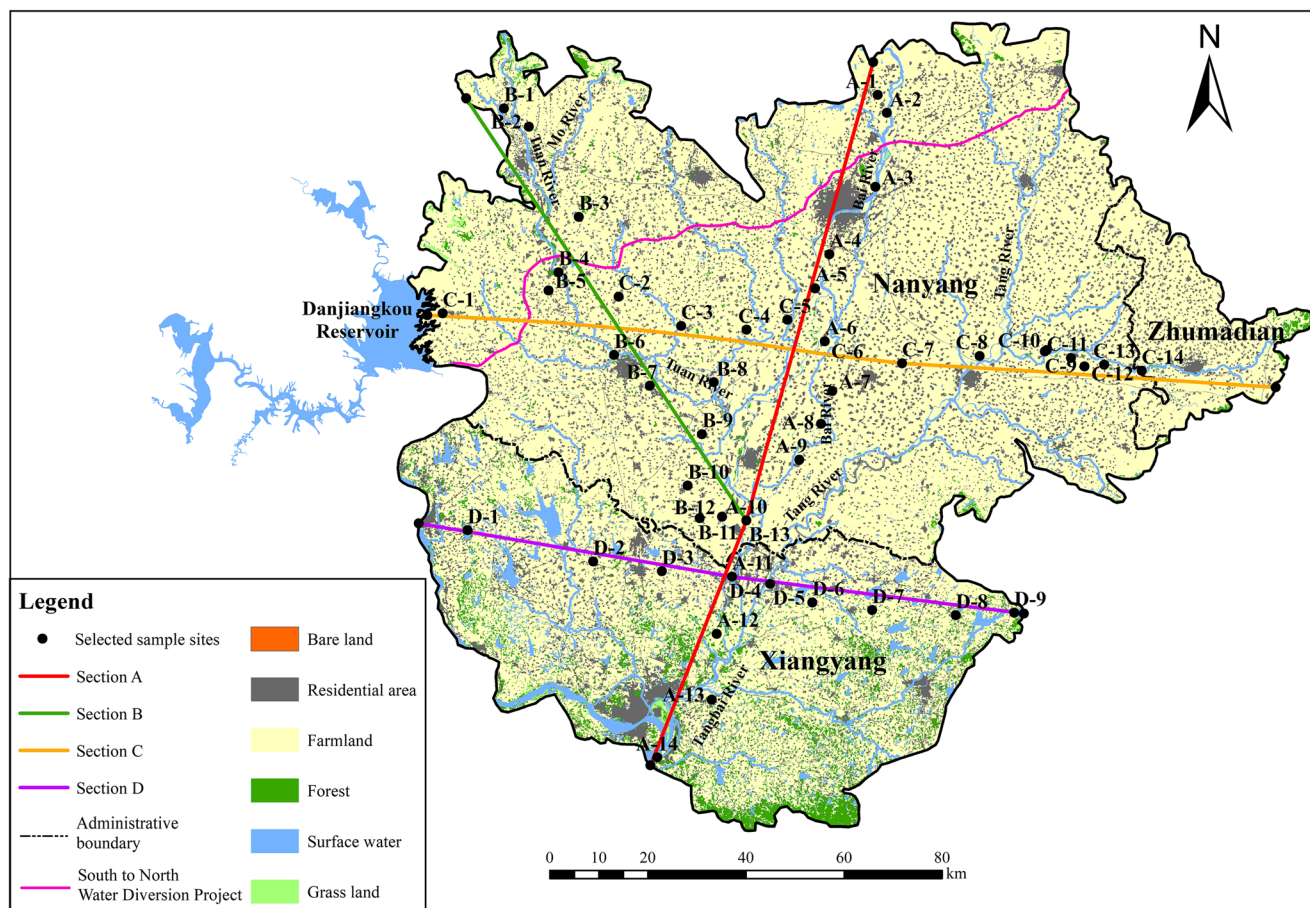
Fig. 2 Land use pattern of the study area in 2015, the arrangement of the four sections used for hydrogeochemical analysis, and sampling locations along these sections

using a laser absorption water-vapor isotope analyzer (Picarro-i2120, CA, USA).

The measurements of $\delta^{15}N$-NO_3^- and $\delta^{18}O$-NO_3^- were carried out at the Chinese Academy of Agricultural Sciences, using the denitrified method based on the isotopic analysis of the nitrous oxide (N_2O) produced by the denitrifying bacterium *Pseudomonas aureofaciens* (Sigman et al. 2001). The produced N_2O was concentrated and purified on a trace gas system, and the isotopic composition was determined using an isotope ratio mass spectrometer (Thermo-Finnigan, USA). During the measurement of $\delta^{15}N$, USGS34 potassium nitrate (KNO_3, $\delta^{15}N = -1.8 \pm 0.2‰$) and USGS32 KNO_3 ($\delta^{15}N = +180 \pm 0.1‰$), standards were used to correct the values obtained. For $\delta^{18}O$ measurement, the samples were referenced using USGS34 ($\delta^{18}O = +27.9 \pm 0.6‰$) and USGS35 sodium nitrate ($NaNO_3$, $\delta^{18}O = +57.5 \pm 0.6‰$) standards.

The stable isotope ratios are expressed in delta (δ) units and a per mil (‰) notation relative to an international standard. The $\delta^{15}N$ values are reported relative to N_2 in atmospheric air (AIR), whereas the $\delta^{18}O$ and δD values are reported relative to Vienna Standard Mean Ocean Water (VSMOW). The uncertainty (2σ) values for $\delta^{18}O$-H_2O and δD-H_2O were ± 0.1 and

$\pm 1‰$, respectively. The precision for $\delta^{15}N$-NO_3^- is 0.4‰, whereas that for $\delta^{18}O$-NO_3^- is 1.6‰ (VSMOW). All statistical analyses were carried out using the software package SPSS 26 (IBM Corp. Released 2019). The isotopic values (δ notation) were calculated via Eq. (1):

$$\delta \; sample \; (‰) = (R \; sample - R \; standard)/R \; standard \times 1000, \qquad (1)$$

where $R = D/H$, $^{15}N/^{14}N$, or $^{18}O/^{16}O$. The $^{15}N/^{14}N$ values were reported relative to atmospheric air, and the D/H and $^{18}O/^{16}O$ values were reported relative to Vienna Standard Mean Ocean Water.

Bayesian isotopic mixing model

Based on qualitative deduction using the values of $\delta^{15}N$-NO_3^- and $\delta^{18}O$-NO_3^-, the contributions of groundwater nitrate sources were quantified using the Bayesian isotopic mixing model (Parnell et al. 2010; Yang et al. 2013). Four potential sources were taken into consideration, based on the results of field survey and land use analyses: sewage and manure (SAM), atmospheric deposition (AD), synthetic fertilizer (SF), and soil nitrogen (SN). The basic equations of SIAR

are as follows:

$$X_{ij} = \sum_{k=1}^{k} P_k q_{jk} \left(S_{jk} + C_{jk} \right) + \varepsilon_{jk} \tag{2}$$

$$S_{jk} \sim N \left(\mu_{jk}, \omega_{jk}^2 \right) \tag{3}$$

$$C_{jk} \sim N \left(\lambda_{jk}, \tau_{jk}^2 \right) \tag{4}$$

$$\varepsilon_{jk} \sim N \left(0, \sigma_j^2 \right) \tag{5}$$

where X_{ij} is the isotope value j of the mixture i, in which $i = 1,2,3,\ldots$, N, and $j = 1, 2, 3,\ldots$, J; S_{jk} is the source value k on isotope j ($k = 1, 2, 3,.,$ K) and is normally distributed with mean μ and standard deviation ω; P_k is the proportion of source k which needs to be estimated by the SIAR model; C_{jk} is the fractionation factor for isotope j on source k and is normally distributed with mean λ and standard deviation τ; and ε_{ij} is the residual error representing the additional unquantified variation between individual mixtures and is normally distributed with mean = 0 and standard deviation σ.

Multivariate data analysis

Due to the distribution of most chemical data failed to meet the assumption of normality for parametric statistical analyses, the non-parametric Kruskal–Wallis test was used to analyze the differences of major ions concentration and isotopic compositions among different land use type (Zhang et al. 2018a; Torres-Martínez et al. 2021). The linear regression analyses and Spearman correlation coefficient were also used to determine the relation between major ions (Menció et al. 2016). All statistical analyses were supported by SPSS version 26 and Microsoft Excel.

Results

Hydrochemical characteristics of groundwater

Table 1 shows the descriptive statistics of major ions and in situ measurements. The concentration of NO_3^- ranged from below the detection limit to 1001 mg L^{-1}, with an average of 102.95 mg L^{-1}. The standard deviation of nitrate was 159.89 mg L^{-1}, which was the second highest among all ions. The average levels of Ca^{2+} and HCO_3^- were 129.08 and 325.88 mg L^{-1}, respectively; they were the main ions. Evapotranspiration is not the main factor determining water chemistry (Gibbs diagrams as Fig. S1.a and Fig. S1.b in Supplemental Material). Therefore, the values of EC, TDS, Na^+, and Cl^- are likely to be influenced by water–rock interactions and anthropogenic activities. The standard deviations of EC and TDS were 816 μS/cm and 554.25 mg L^{-1}, respectively, suggesting point source contamination, such as sewage

outfalls or septic tanks, may greatly influence the groundwater compositions near the corresponding sampling sites. This assumption is supported by the statistics of Cl^- and Na^+, with average values of 87.20 and 55.15 mg L^{-1}. However, due to farmland being the main land use type, the application of fertilizer is ubiquitous in the study area. Whether the point source and non-point sources coexist and the relationship between them remain for further discussions.

According to the analysis of all 160 samples, $Ca-HCO_3$ was the most representative chemical compound of groundwater in the Nanyang Basin (38%), followed by $Ca-HCO_3-Cl$ and $Ca-Na(K)-HCO_3$ (11.85% and 11.25%, respectively) and by $Ca-Mg-HCO_3$ (8.12%). Other types of compounds were combinations of the above ions (Table S3). The quantity of each type was less than 7, probably as a result of strong mixing effects and anthropogenic activities. We generated a Piper diagram to highlight the different water facies in the study area (Fig. 3). The proportion of Mg^{2+} was generally stable for both shallow and deep aquifers. In most of the samples from the shallow aquifer, Ca^{2+} was the major cation and the Na^+ was mostly below 40%. Generally, HCO_3^- was the major anion, although in some samples from the residential area, Cl^- was abundant, suggesting point source pollution. The sample distribution of the deep aquifer was more dense than that of the shallow aquifer; Ca^{2+} and HCO_3^- were also the major ions.

According to Table 2, TDS and EC highly correlate with almost all ions except NO_2^-. Ca^{2+} showed the highest correlation with TDS and EC. Although HCO_3^- had higher mean concentrations compared to SO_4^{2-} and Cl^-, its correlations with the main cations, such as Ca^{2+}, Mg^{2+}, and Na^+, were all weaker than those with SO_4^{2-} and Cl^-. Nitrate was strongly correlated with TDS, Ca^{2+}, Mg^{2+}, and Na^+.

Nitrate concentrations in different land use types

The average concentration of NO_2^- was 0.05 mg L^{-1}, far below the average of NO_3^-. Although we determined NH_4^+ for each sample, the values are not included in Table 1 as they were mostly below the detection limit. Hence, nitrate was the major form of dissolved inorganic nitrogen in the study area.

Based on our results, Cl^- was significantly correlated with NO_3^-. Samples in different land use had significantly different NO_3^- and Cl^- concentrations ($p = 0.008$ and 0.049, respectively). Samples of surface water had the lowest concentrations and the narrowest distribution. Samples from the residential area had the highest concentrations of Cl^- and NO_3^-, with average levels of 114.43 mg L^{-1} and 162.83 mg L^{-1}, respectively (Fig. 4), and the highest number of outliers. Farmland had the second highest NO_3^- concentrations, ranging from below the detection limit to 784 mg L^{-1}, with an average of 75.71 mg L^{-1} (Table 1). NO_3^- concentration between farmland and residential area was significantly different

Table 1 Descriptive statistics of major indices for different land use types in the Nanyang Basin in China

|	All samples (n = 160)				Farmland (n = 88)				Residential area (n = 57)				Forest (n = 7)				Surface water (n = 7)			
	Min	Max	Mean	Sd	Min	Max	Mean	Sd	Min	Max	Mean	Sd	Min	Max	Mean	Sd	Min	Max	Mean	Sd
pH	6.5	8.9	7.3	0.37	6.5	8.5	7.36	0.34	6.5	7.8	7.22	0.32	7.2	7.6	7.44	0.17	7.2	8.9	8.02	0.61
EC (μS/cm)	243	5500	1076	816	311	5500	1004	789	438	4720	1284	890	612	1900	997	435	243	636	435	151
ORP (mv)	−37.7	461.7	220.6	64.9	−37.7	427.4	221.4	69.5	83.3	461.7	224.4	61.0	61.5	266.4	205.7	72.6	169.7	223.9	197.4	18.6
DO (mg L^{-1})	4.3	12.4	8.28	1.18	5.2	10.0	8.20	1.10	4.3	9.7	8.13	1.16	7.7	9.2	8.56	0.48	8.6	12.4	10.11	1.56
TDS (mg L^{-1})	140.0	3571.2	686.97	554.25	199.9	3571.2	642.94	534.65	140.0	3108.5	815.82	612.54	439.1	1266.5	646.49	288.17	146.5	404.9	273.49	95.04
Ca^{2+} (mg L^{-1})	16.6	688.6	129.08	97.93	16.6	688.6	118.60	88.71	24.3	550.9	157.41	114.09	75.9	194.6	114.11	39.15	26.7	67.7	52.53	15.24
Mg^{2+} (mg L^{-1})	5.8	180.2	29.43	25.09	8.8	146.8	28.15	23.81	5.8	180.2	33.26	28.59	17.3	66.2	33.85	15.53	7.3	16.2	11.65	2.69
Na$^+$ (mg L^{-1})	3.4	393.8	55.15	51.17	3.4	393.8	55.91	57.86	10.0	186.0	58.32	43.81	34.6	126.7	58.32	33.05	4.8	41.8	19.70	13.51
K$^+$ (mg L^{-1})	0.2	96.5	3.89	10.12	0.27	96.5	3.52	11.14	0.2	52.6	3.73	8.16	0.4	42.5	8.11	15.39	1.8	14.4	6.07	4.96
HCO$_3^-$ (mg L^{-1})	86.7	871.4	325.88	120.39	126.9	871.4	333.50	124.54	116.0	546.1	330.71	104.98	209.9	558.9	367.43	114.09	86.7	190.4	144.09	37.91
SO$_4^{2-}$ (mg L^{-1})	5.8	1794.9	90.12	157.89	5.8	1794.9	91.44	201.96	5.8	340.6	92.25	79.92	40.4	284.3	96.06	85.76	34.6	85.5	59.97	17.78
Cl$^-$ (mg L^{-1})	3.5	755.8	87.20	115.76	3.6	755.8	76.12	104.22	3.5	677.8	114.43	138.93	33.0	171.9	76.93	52.88	7.1	52.1	26.79	17.10
NO$_3^-$ (mg L^{-1})	BDL	1001.0	102.95	159.89	BDL	784.0	75.71	102.70	0.4	1,001.0	162.83	223.39	10.7	99.9	55.65	36.25	7.1	33.3	16.15	10.68
NO$_2^-$ (mg L^{-1})	BDL	0.72	0.05	0.11	BDL	0.72	0.05	0.13	BDL	0.5	0.03	0.09	BDL	BDL	BDL	BDL	BDL	0.3	0.11	0.13
Fe (mg L^{-1})	BDL	25.2	0.50	2.15	BDL	25.2	0.58	2.79	BDL	5.4	0.40	0.97	BDL	1.3	0.38	0.53	BDL	0.6	0.35	0.20
Mn (mg L^{-1})	BDL	5.4	0.16	0.63	BDL	4.9	0.16	0.06	BDL	5.4	0.02	0.75	BDL	0.2	0.05	0.07	BDL	0.3	0.11	0.11

n sample number

BDL below the detection limit
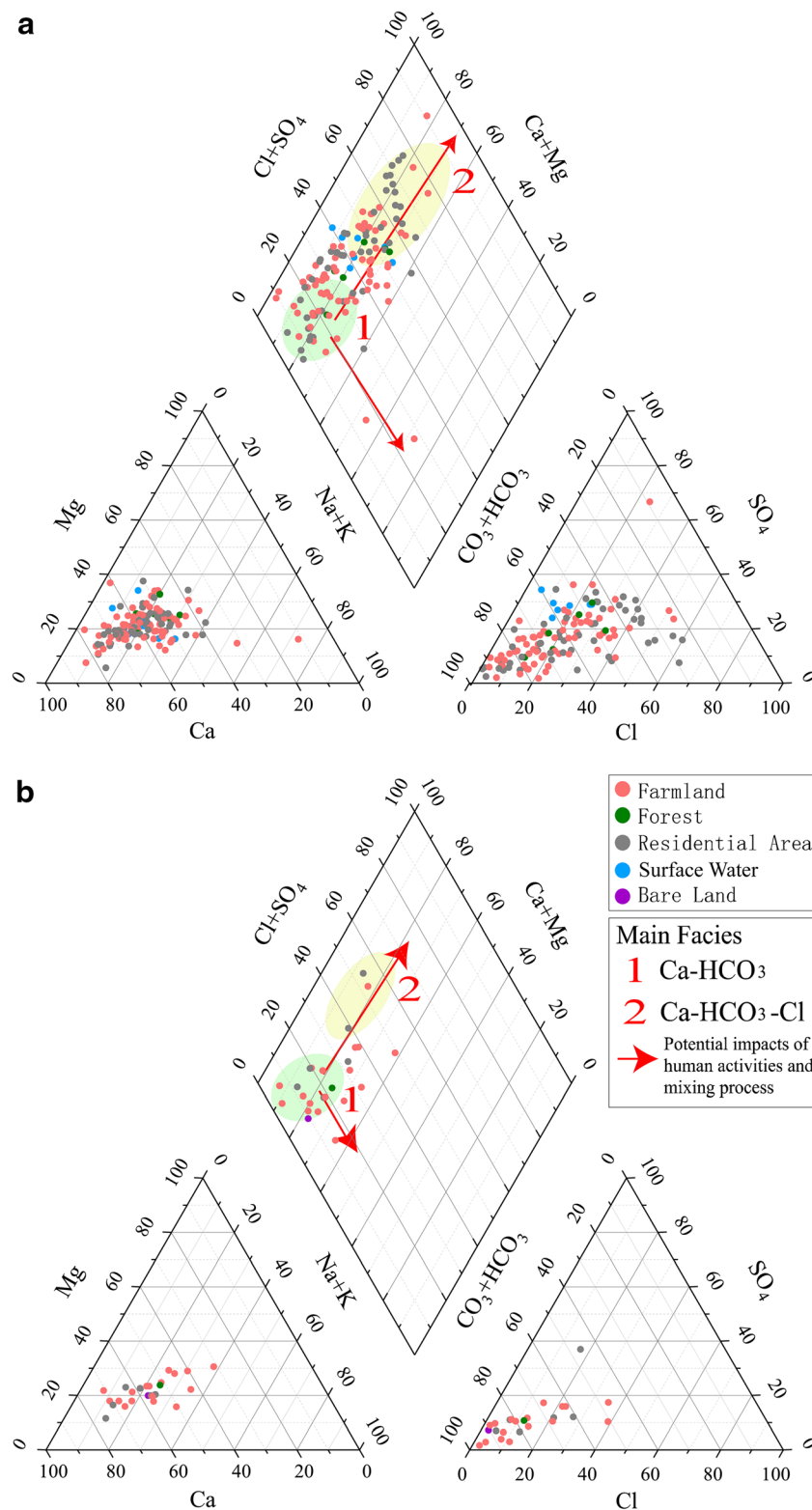
Fig. 3 Piper diagrams of different land uses in shallow and deep aquifers. (a) Piper diagram for samples of the shallow aquifer and surface water, (b) Piper diagram for samples of the deep aquifer

($p = 0.017$); however, difference of Cl^- concentration between these two groups was insignificant ($p = 0.072$). Forest samples showed concentration range similar to that of farmland

samples, with NO_3^- and Cl^- concentrations ranging from 10.7 to 99.9 mg L^{-1} and 33.0 to 171.9 mg L^{-1}, respectively. Further details and discussions between Cl^- and NO_3^- were

Table 2 Correlation matrix of major ions in groundwater of the Nanyang Basin in China

	pH	EC	ORP	DO	TDS	Na$^+$	K$^+$	Ca^{2+}	Mg^{2+}	HCO$_3^-$	SO$_4^{2-}$	Cl$^-$	NO$_3^-$	NO$_2^-$	Fe	Mn
pH	1															
EC	− 0.140	1														
ORP	0.087	0.076	1													
DO	0.465**	0.044	0.169*	1												
TDS	− 0.105	0.982**	0.111	0.075	1											
Na$^+$	− 0.079	0.763**	0.075	0.066	0.786**	1										
K$^+$	0.125	0.368**	0.091	0.116	0.387**	0.438**	1									
Ca^{2+}	− 0.128	0.953**	0.133	0.066	0.966**	0.659**	0.295**	1								
Mg^{2+}	− 0.136	0.904**	0.099	0.035	0.910**	0.762**	0.333**	0.830**	1							
HCO$_3^-$	− 0.003	0.491**	0.137	− 0.060	0.510**	0.489**	0.400**	0.484**	0.520**	1						
SO$_4^{2-}$	− 0.001	0.747**	0.065	0.096	0.752**	0.574**	0.304**	0.739**	0.659**	0.246**	1					
Cl$^-$	− 0.172*	0.928**	0.079	0.048	0.929**	0.736**	0.310**	0.893**	0.897**	0.400**	0.607**	1				
NO$_3^-$	− 0.114	0.765**	0.099	0.083	0.794**	0.577**	0.212**	0.774**	0.684**	0.252**	0.301**	0.756**	1			
NO$_2^-$	0.078	0.177*	− 0.161*	0.064	0.183*	00.116	− 0.039	0.171*	0.165*	0.069	0.338**	0.086	− 0.003	1		
Fe	− 0.105	− 0.036	− 0.299**	0.044	− 0.028	− 0.030	− 0.033	− 0.052	− 0.003	− 0.127	0.015	0.061	− 0.080	− 0.012	1	
Mn	− 0.104	0.013	− 0.221**	− 0.012	0.000	− 0.004	− 0.043	− 0.021	0.070	0.045	0.035	0.048	− 0.090	0.309**	0.620**	1

**Correlation is significant at the 0.01 level (2-tailed)

*Correlation is significant at the 0.05 level (2-tailed)

Dissolved oxygen (DO) and total dissolved solids are in mg L^{-1}. Oxidation–reduction potential (ORP) is in mV, and electrical conductivity (EC) is in µS/cm
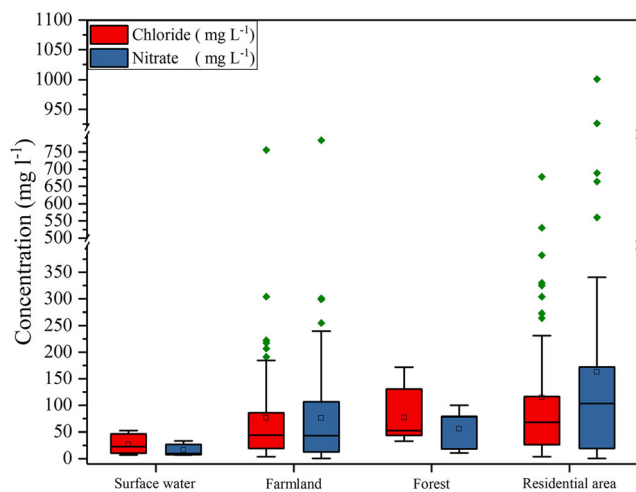
Fig. 4 NO_3^- and Cl^- concentrations of different land use types in the Nanyang Basin in China

included in "Relationships between hydrochemistry and nitrate sources."

Different parts of the Nanyang Basin show different hydrogeological conditions, population densities, and agricultural and industrial structures. Because of this, we selected four sections (Fig. 2). Sections A and B ran through the entire study area from north to south, converging with each other at A-10 (B-13). These two sections represented the main channel of the Tuan River and the Bai River, respectively, and are both tributaries of the Tangbai River. Sections C and D were east–west sections; the starting point of section C (e.g., C-1) was near the Danjiangkou reservoir, the origin of the SNWDP.

According to Table 3 and Fig. 5, for two north-to-south sections (sections A and B), the average NO_3^- levels did not exceed the average of the entire study area. Section A had the lowest average values for both NO_3^- and Cl^-. The relatively low concentrations of ions alongside major river indicate surface water mixing and, consequently, the dilution of the ion concentrations in the groundwater. Hyporheic zones, which

are located on both sides of the river channel, may have also significantly contributed toward the reduction of nitrate through denitrification (Kim et al. 2018; Meghdadi and Javar 2018b). For sections C and D, which run through the study area from east to west, with a small amount of water bodies, the concentrations of NO_3^- and Cl^- were higher, most likely because of the absence of dilution caused by hyporheic zones and surface water (Huizenga et al. 2017). We collected nine samples from section D, and their mean concentrations were the highest among all four sections. However, according to Fig. 5d, the concentrations of NO_3^- and Cl^- for D-2 were abnormally high, suggesting the existence of strong point source contamination sample. For the other eight samples, D-1 had the highest concentrations, with 125.03 and 86.85 mg L^{-1} for NO_3^- and Cl^-, respectively. The values for D-3 to D-9 were below the overall mean values.

Stable isotope composition of nitrate

As shown in Fig. 6, we collected 28 water samples from the selected nitrate-contaminated area to measure the concentrations of the main ions and to analyze isotopic composition (Table S4). Similar to the data obtained for the whole basin, Ca^{2+} and HCO_3^- were the major cations and anions, and there were no significant differences for these two ions between two sampling campaign ($p = 0.092$ and 0.596, respectively). Cl^- and NO_3^- showed similar ranges for these two sampling campaign ($p = 0.967$ and 0.211 for Cl^- and NO_3^-, respectively). The average Cl^- and NO_3^- levels are 74.60 ± 78.73 mg L^{-1} and 102.97 ± 101.59 mg L^{-1}, respectively (mean ± SD, detailed data are shown in Table S4).

According to Fig. 9, the stable isotope composition of nitrate ranges from 3.88 to 18.64‰ (average 10.92 ± 3.63‰) for $\delta^{15}N\text{-}NO_3^-$ and from −0.43 to 7.09‰ (average 3.42 ± 1.97‰) for $\delta^{18}O\text{-}NO_3^-$. No simple correlations were observed

Table 3 NO_3^- and Cl^- average concentrations of different land use types along the four sections

Class	Land use type	Section A (n = 14)		Section B (n = 13)		Section C (n = 14)		Section D (n = 9)	
		NO_3^-	Cl^-	NO_3^-	Cl^-	NO_3^-	Cl^-	NO_3^-	Cl^-
Surface water (n = 5)	Surface water (n = 5)	9.64	20.92	27.03	39.88	8.61	22.69	26.55	46.79
Shallow aquifer (n = 34)	Residential area (n = 13)	55.70	59.20	154.59	114.15	141.85	111.67	53.79	45.26
	Farmland (n = 20)	73.08	63.61	90.88	73.83	113.44	77.34	265.12	260.56
	Forest (n = 1)	-	-	-	-	-	-	78.69	52.11
Deep aquifer (n = 11)	Residential area (n = 3)	-	-	14.11	7.09	243.85	95.72	-	-
	Farmland (n = 7)	73.97	75.27	87.25	63.46	56.89	90.40	-	-
	Forest (n = 1)	-	-	-	-	-	-	18.28	32.97
Average		65.01	62.11	83.39	66.05	115.31	86.42	120.03	116.59

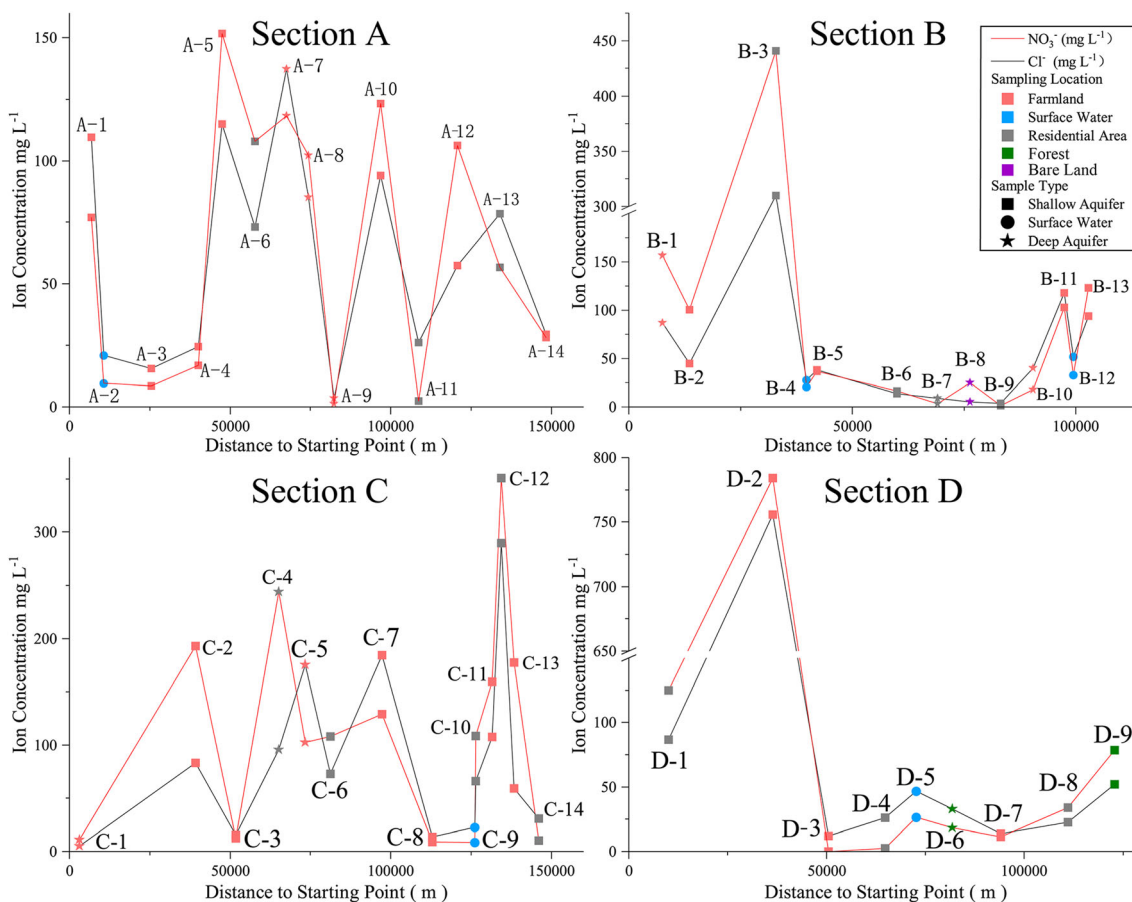Hyphen "-" means only no sample of specific category

Fig. 5 Ion concentrations along the four hydrochemical sections. The red and black lines indicate changes in NO_3^- and Cl^-, respectively, along each section

between $\delta^{15}N–NO_3^-$ or $\delta^{18}O–NO_3^-$ versus concentrations of NO_3^- (Fig. S2 and Fig. S3 in Supplemental Material).

Discussion

Relationships between hydrochemistry and nitrate sources

The Gibbs plot identifies the influences of water–rock interactions, evaporation, and precipitation on water chemistry (Feth and Gibbs 1971). Most samples were taken from the water–rock interaction zone (Fig. S1.a and Fig. S1.b). This finding was consistent with the local meteorological and hydrogeological features. However, some samples were outside the typical ranges, indicating the influence of anthropogenic activities.

The contributions of water–rock interaction and anthropogenic activities to groundwater could be further differentiated by the $[Na^++K^+]/[HCO_3^-]$ versus $[Ca^{2+}+Mg^{2+}]/[HCO_3^-]$ diagram (Fig. 7). Water samples close to the $[Na^++K^+]/[HCO_3^-] = 0$ and $[Ca^{2+}+Mg^{2+}]/[HCO_3^-] = 1$ were affected by the weathering of carbonate minerals, whereas samples along

the $[Ca^{2+}+Mg^{2+}+Na^++K^+]/[HCO_3^-] = 1$ line suggest contribution of the dissolution of silicate minerals. According to Fig. 7, a large part of the samples was located in quadrant B, related to groundwaters with an excess of cations $(Ca^{2+}+ Mg^{2+}+Na^++K^+)$ over HCO_3^-, which cannot be ascribed to any of the abovementioned water–rock interactions. Therefore, anthropogenic activities can explain such cation enrichment (Buccianti et al. 2014; Gibrilla et al. 2020). This leads us to infer that NO_3^-, K^+, Na^+, and Cl^- are mostly derived from agricultural fertilizers, animal waste, and municipal and industrial sewage, altering the chemical composition of the water.

Elevated concentrations of Na^+ and Cl^- are usually a result of the sewage and manure (SAM) inputs, although some synthetic fertilizers may also contain trace amounts of Cl^-. The addition of potassium chloride or calcium chloride to synthetic fertilizer has also been reported (Bakeer 2016; Oberhelman and Peterson 2020). The dissolution of halite could be another potential reason for the increasing of Na^+ and Cl^-, which would cause Na^+/Cl^- molar ratio to be 1:1.

The application of deicing agents in the study area could be eliminated as a potential source of Na^+ and Cl^- in the study area since the annual mean temperature is 16.8 °C and the
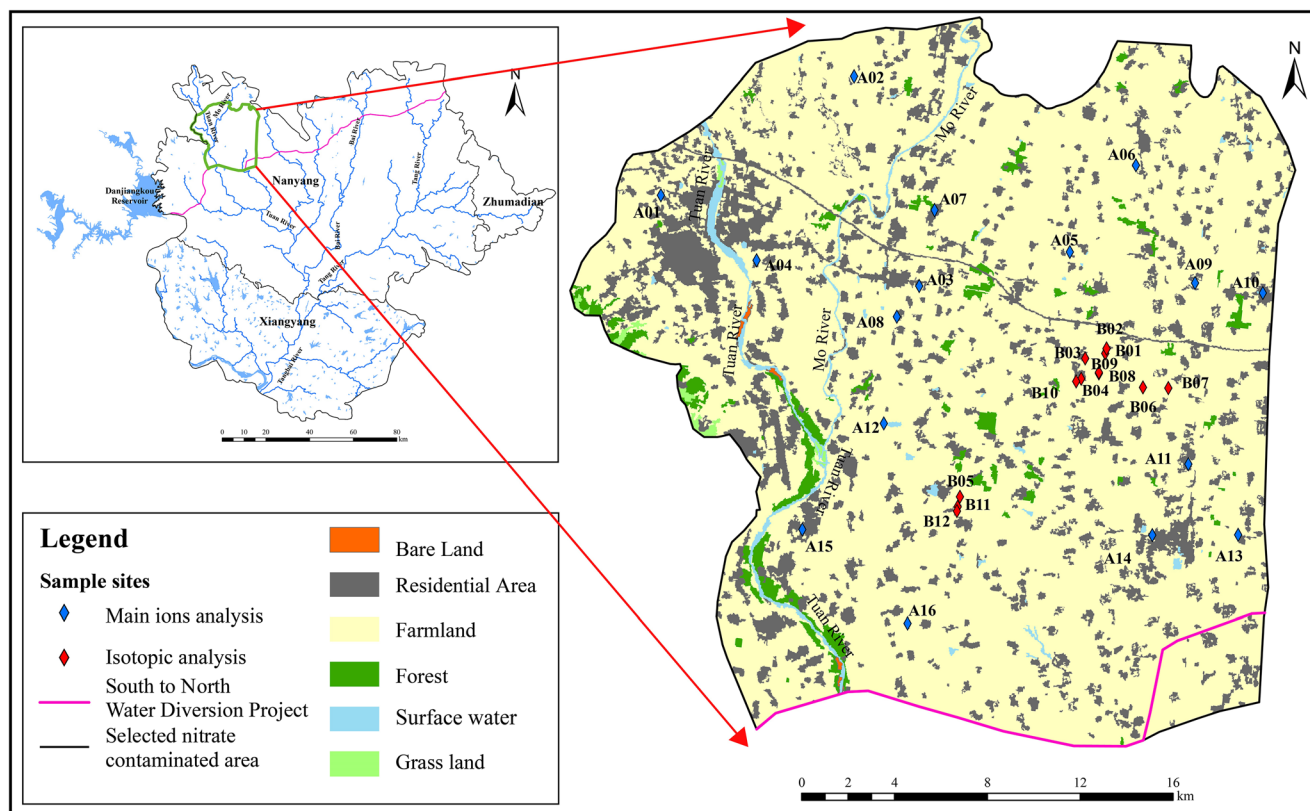
Fig. 6 Location of the selected typical nitrate-contaminated area in in the Nanyang Basin

main land use type in our study area is farmland (Fig. 2 and Table S2). According to Fig. 8b, for samples in residential area, with the increasing of Na^+ concentration, more samples were located above the 1:1 line ($R^2 = 0.78$, $p < 0.01$), suggesting there were additional Cl^- compared with Na^+. The potential source for excessive Cl^- should be sewage and manure since Na^+ was rarely used as synthetic fertilizer (Roy et al.

Fig. 7 Binary plot as $[Na^+ + K^+]/[HCO_3^-]$ vs. $[Ca^{2+}+Mg^{2+}]/[HCO_3^-]$ as equivalent ratios

1999). Samples in forest had an almost 1:1 Na^+/Cl^- molar ratio ($R^2 = 0.79$, $p < 0.01$), indicating that the dissolution of halite was the main cause of Cl^- in the relatively natural conditions. The slope of linear fitting line for farmland was also close to 1 ($R^2 = 0.78$, $p < 0.01$), suggesting the applied of chloride contained fertilizer was limited and did not influence the concentration of Cl^- in the study area. According to the distribution of all samples, it was noteworthy that Na^+ was more than Cl^- when concentration was less than 4 mmol/L. It was reported that Na^+ is a major component of N containing organic effluents (Minet et al. 2017; Guo et al. 2020). Furthermore, the incongruent dissolution of Na-K silicate minerals can also cause the excess of Na^+ relative to Cl^- (Buccianti et al. 2014).

Chloride in the water can indicate sewage and manure inputs. Due to the impacts of anthropogenic sources of nitrogen (Table 2), a significant positive correlation ($p < 0.01$) was observed between Cl^- and NO_3^- ($r = 0.756$). Therefore, the NO_3^-/Cl^- method can provide more information to help distinguish the effect of N removal processes by dilution from denitrification (Chen et al. 2014; Widory et al. 2005). Domestic effluent is characterized by a low NO_3^-/Cl^- ratio and a high Cl^- concentration (Lu et al. 2015). On the contrary, samples influenced by synthetic fertilizer would have high NO_3^-/Cl^- ratios with relatively low Cl^- concentrations. With little impacts from water–rock interactions, the NO_3^-/Cl^- method was suitable to distinguish the influences of SAM
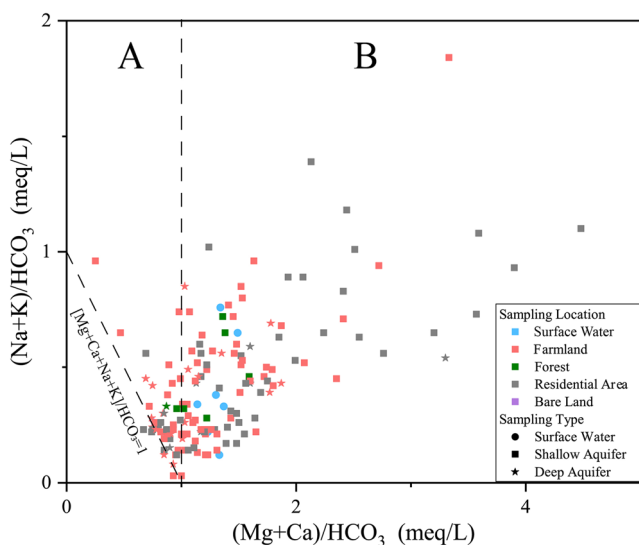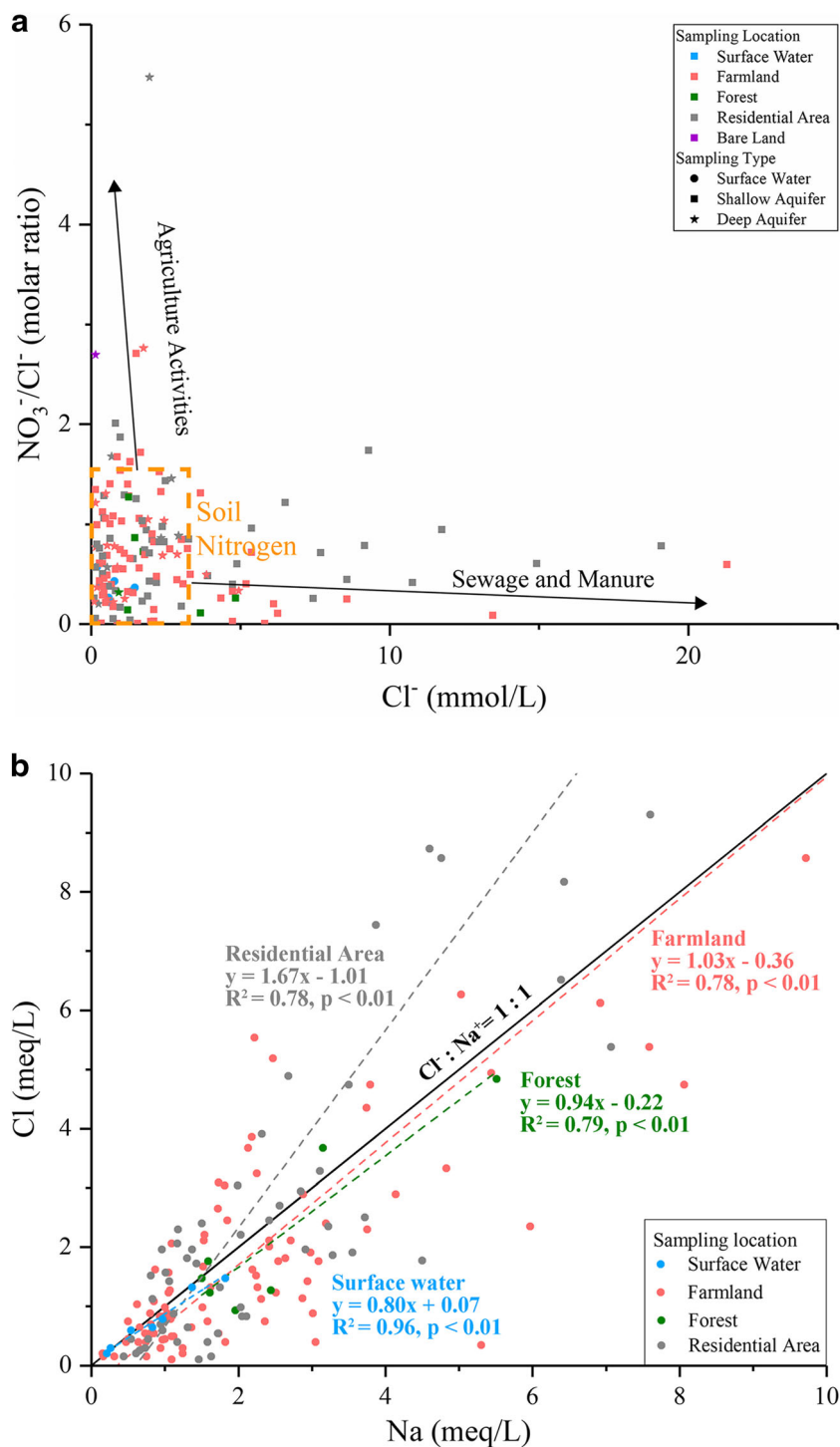
Fig. 8 (a) Scatter plot of NO_3^-/Cl^- molar rate vs. Cl^- mmol concentration; (b) scatter plot of $[Cl^-]$ vs. $[Na^+]$. Note that the linear regression lines with linear fitting equations in same color were shown for samples in different land use types. And the black line denoted the dissolution of halite

from those of SF. The average NO_3^-/Cl^- ratio levels for residential area and farmland are 0.83 and 0.71, respectively (Table S5). Although samples in residential area and farmland had similar NO_3^-/Cl^- levels, both ion concentrations were larger in residential area than in farmland (Table 1), suggesting the mixing of the shallow aquifer. Compared with samples of surface water, the average NO_3^-/Cl ratio was 0.37, indicating that SAM was the main nitrate source for surface water.

Furthermore, many samples were concentrated in the lower left part of Fig. 8a. The low NO_3^-/Cl^- ratio with low Cl^- concentration indicates that these samples were probably influenced by soil nitrogen (SN) (Guo et al. 2020; Torres-Martínez et al. 2021). The mixing of different nitrate sources and high nitrification rate may also cause this situation.

According to the results of our field investigation, synthetic fertilizers are widely used in the study area. In contrast, the use

of organic fertilizers is limited (Nanyang Municipal Government 2019). Nitrate was the main form of DIN, and high levels of NO_3^- in groundwater are often attributed to NO_3^- transport via leaching (Li et al. 2019; Meybeck 1982). Nitrate does not form any insoluble minerals that could precipitate or are easily adsorbed via aquifer pores. For most of the samples, the pH ranged between 7 and 8, whereas the DO was in the range of 4.3 to 12.4 (Table 1). Most surface water samples had a pH above 8 and high DO values (10.11 mg L^{-1}). During the leaching process, with decreasing DO and pH levels, the concentration of NO_3^- increased, indicating that the shallow aquifer had acidic conditions.

Nitrate dynamics and source identification using isotope data

Most of the samples were within the range of SAM (typically from 5.2 to 25‰), and some were in the overlapping zone between SN and SAM, demonstrating the mixing effects of different sources. Only one sample was located in the overlapping zone of synthetic fertilizer and soil N (Fig. 9).

The $\delta^{18}O$-NO_3^- level of nitrate derived from microbial ammonium nitrification can be calculated by Eq. (6), where the expected $\delta^{18}O$-NO_3^- is only the expected value when nitrification occurs. Here, $\delta^{18}O$-H_2O is the $\delta^{18}O$ value in the water and $\delta^{18}O$-O_2 is the $\delta^{18}O$ value in the air. Although the calculation using Eq. (6) can lead to unreliable results, it is generally acknowledged that the NO_3^- produced by nitrification has distinct $\delta^{18}O$–NO_3^-, determined by the $\delta^{18}O$ of H_2O and by atmospheric O_2 (Hinshaw et al. 2020). In theory, two oxygen atoms of the newly formed NO_3^- are derived from

H_2O oxygen, and the third oxygen atom is incorporated from atmospheric O_2 (Mayer et al. 2001). Five samples of $\delta^{18}O$-H_2O were measured in our study, resulting in an average value of − 7.22‰. According to a previous study near the Nanyang Basin (Du et al. 2017), the $\delta^{18}O$-O_2 resulting from atmospheric O_2 is 23.5‰. Based on the above assumptions, the theoretical $\delta^{18}O$-NO_3^- line was plotted (Fig. 9). Equation (6) is as follows:

Expected $\delta^{18}O_{nitrate} = 1/3\ \delta^{18}O - O_2 + 2/3\ \delta^{18}O - H_2O$ (6)

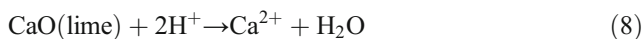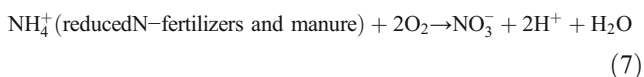Except for the two samples with the highest and lowest $\delta^{15}N$-NO_3^- values, other samples were located near the line of estimated nitrification. The range of $\delta^{18}O$-NO_3^- also suggests high bioactivity in the unsaturated zone. Most of the nitrate in the study area was a result of microbial activity, with nitrification being the dominant leaching process (Minet et al. 2012). Although synthetic fertilizers are widely used, no samples fell into the "NO_3^- fertilizer" category.

Due to the mineralization-immobilization turnover (MIT) process, there is a complex exchange mechanism between $\delta^{18}O$-H_2O and $\delta^{18}O$-O_2. Large gross rates of NO_3^- immobilization by bacteria are followed by rapid remineralization (Mengis et al. 2001), and the hypothesis that crops preferentially take up nitrate while ammonia remains for nitrification would mask the original high $\delta^{18}O$-NO_3^- values (Roadcap et al. 2002). For the above reasons, the composition of $\delta^{18}O$-NO_3^- is not identical to that concluded based on laboratory conditions (Kendall et al. 2000). These findings suggest a possible limitation of DIM in identifying the contribution of nitrate fertilizers (Minet et al. 2012; Spalding et al. 2018a, 2018b).

Fig. 9 Relationship between $\delta^{18}O$- NO_3^- and $\delta^{15}N$- NO_3^- in a selected part of the study area. The range of isotopic composition derived from (Ding et al. 2015), (Xue et al. 2009) and (Yang et al. 2013)
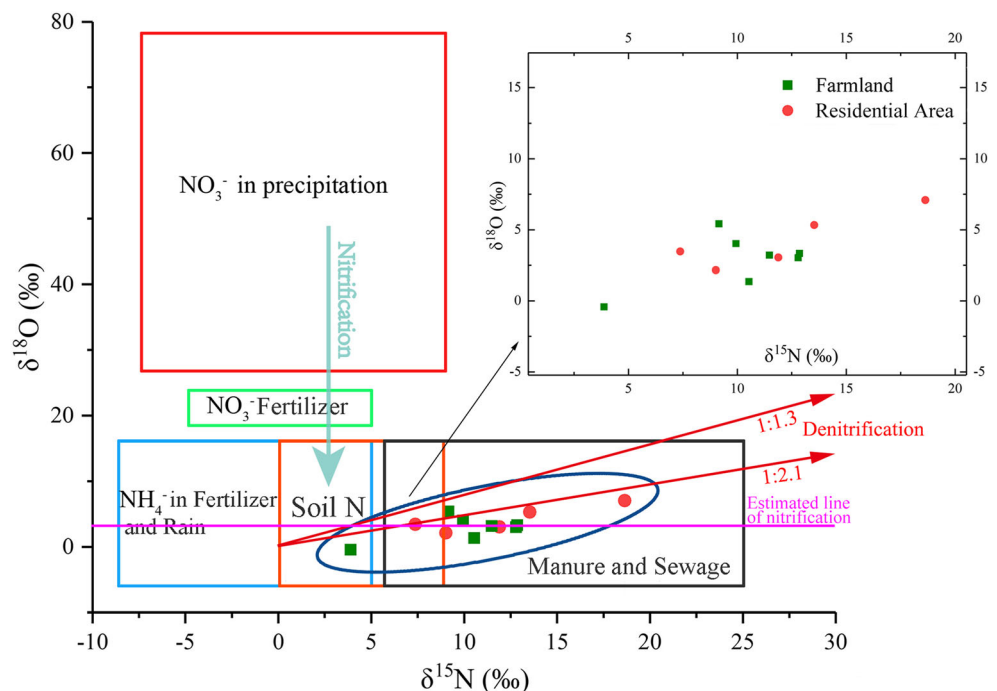
According to Fig. 3, Ca^{2+} was the main cation in groundwater. By the analysis of the relationship between $[Ca^{2+} + Mg^{2+}] - [HCO_3^- + SO_4^{2-}]$ and $[Na^+ - Cl^-]$ (Fig. S4 in Supplemental Material), there were potential additional sources of Ca^{2+} and Mg^{2+} besides the dissolution of carbonate mineral (e.g., calcite/dolomite) and evaporite (e.g., gypsum and anhydrite). Therefore, besides the strong water–rock interactions identified by Gibbs diagram (Fig. S1 and Fig. S2 in Supplemental Material), Eqs. (7) and (8) could represent the influences caused by nitrification to hydrochemical evolution due to anthropogenic activities (Kim et al. 2009). Equations (7) and (8) are as follows:

$$NH_4^+ (reduced N-fertilizers\ and\ manure) + 2O_2 \rightarrow NO_3^- + 2H^+ + H_2O \tag{7}$$

$$CaO(lime) + 2H^+ \rightarrow Ca^{2+} + H_2O \tag{8}$$

Denitrification is a nitrate removal process which causes $\delta^{15}N\text{-}NO_3^-$ and $\delta^{18}O\text{-}NO_3^-$ to increase linearly over a wide range of values along a slope between 0.5 and 0.8 (Granger and Wankel 2016). However, the flat slope of $\delta^{18}O\text{-}NO_3^-$ vs. $\delta^{15}N\text{-}NO_3^-$ in Fig. 9 was not indicative of isotope enrichment during denitrification. According to Table 1, the average DO was 8.23 mg L^{-1}. At DO levels above 2 mg L^{-1}, the aerobic environment will suppress denitrification, and oxygen will be the first electron donor instead of nitrate. In addition, the practical absence of Fe and Mn (mean concentrations of 0.50 and 0.16 mg L^{-1}, respectively) also indicates that denitrification was not significant throughout the study area. For samples from the residential area, the availability of organic carbon in domestic effluent and the leaching of manure or slurries may provide sufficient organic carbon, acting as electron donor to facilitate denitrification in the shallow aquifer (Atekwana and Geyer 2018). Based on our results from the residential area, denitrification may be a secondary process, causing a slight enrichment in $\delta^{15}N\text{-}NO_3^-$ and $\delta^{18}O\text{-}NO_3^-$.

Based on the distribution of all 12 samples, with relatively stable compositions of $\delta^{18}O\text{-}NO_3^-$, $\delta^{15}N\text{-}NO_3^-$ levels were clearly elevated. The stable composition of $\delta^{18}O\text{-}NO_3^-$ suggests that nitrate produced by nitrification was the main nitrate source in the study area. The mixing of different sources between SAM and SF caused the wide distribution of $\delta^{15}N\text{-}NO_3^-$, and the influences of domestic effluent were greater than those of agricultural activities. In this sense, the leachate from SAM may cause $\delta^{15}N\text{-}NO_3^-$ enrichment of the underlying water due to the lateral flow of groundwater (Pasten-Zapata et al. 2014). Organic nitrogen and ammonium are the major nitrogen forms in SAM (Ma et al. 2019; Minet et al. 2012), and both are easily mineralized into nitrate during the leaching process. At the same time, volatilization is the main mechanism that enriches $\delta^{15}N\text{-}NO_3^-$ in SAM to values larger than 10‰. As a result of the mixing between different sources, $\delta^{15}N\text{-}NO_3^-$ levels of samples in farmland were also increased.

Three samples fell into the category "soil organic N". However, considering the high average concentrations of nitrate and chloride in groundwater, it was unrealistic to hypothesize that soil nitrogen alone could cause current level nitrate contamination (Pasten-Zapata et al. 2014). Furthermore, mineralization-immobilization turnover in the unsaturated zone will also increase the contents of organic N. Samples enriched with $\delta^{15}N\text{-}NO_3$ also had higher chloride concentrations (Table S4), proving the contribution of SAM, which was larger than that of SAM. Once discharged into the natural environment, ammonia is volatilized, causing the enrichment of $\delta^{15}N\text{-}NO_3^-$ (Lasagna and De Luca 2019).

Nitrate source apportionment using SIAR

Calculation of the source contributions in the general isotope mixing model is also a significant issue, because the isotopic ranges and values of different end-member sources are uncertain and overlap (Kim et al. 2015). To overcome this problem, this study applied a stable isotope mixing model with the Bayesian framework (SIAR). The results of SIAR are the probability distributions for each source. With the elimination of denitrification (Fig S2 and S3) and relatively limited measurements of nitrate isotopes, the fractionation factor in Eq. (4) is set to zero.

According to field survey and Fig. 9, AD, SAM, SF (ammonium fertilizer), and SN are regarded as four potential nitrate sources. The reasons why nitrate fertilizer was not regarded as potential nitrate sources were as follows: first, the most common types of nitrogen fertilizer used in China including urea, ammonium carbonate, and urea (Ding et al. 2015; Zhang et al. 2018b) and nitrate fertilizer are limited used. Second, nitrate is easier to move with infiltrating water than other nitrogen form; if nitrate fertilizer was widely applied in the study area, $\delta^{18}O\text{-}NO_3^-$ of groundwater samples collected from farmland should be larger than 20‰. According to Fig. 9, our data did not verify this situation; the $\delta^{18}O\text{-}NO_3^-$ for most samples was close to the theriacal nitrification values calculated by Eq. (6).

With the identification of nitrification as the main nitrogen transformation process in the study area, the $\delta^{18}O\text{-}NO_3^-$ of SF and SN were calculated by Eq. (6) (Table S4). Due to the limited number of nitrate isotopes sample ($n = 12$), the range values of $\delta^{15}N\text{-}NO_3^-$ and $\delta^{18}O\text{-}NO_3^-$ could not derive from isotopic composition of samples in our study directly. In order to get reliable results of contribution from different nitrate sources, the most convenient and realistic way under our circumstance was to find these values in relevant literatures (Jin et al. 2018; Zhang et al. 2018b; Li et al. 2019). The reason why these literatures were selected was that their study areas had a similar fertilizer application rates, and so did the climate

characteristics. The isotopes range for four potential nitrate sources is listed in Table 4.

The proportional contribution of four potential nitrate sources is illustrated in Fig. 10. The mean probability estimate (MPE) of different sources was ranked as: SAM > SN > SF >AD (Table S6). SAM was the main nitrate source for Nanyang Basin (MPE 45.41 ± 9.97%); SN (MPE 35.81 ± 15.47%) was the second nitrate source in the study area. The contributions of SF (MPE 17.87 ± 11.95%) were significantly lower than those of SAM and SN. As discussed in "Nitrate dynamics and source identification using isotope data," nitrification and ammonium volatilization were the main nitrogen transformation process in the study area; the contribution of SN was in accordance with the high rate of nitrification in the study area. The high contribution of SN was also rationalized by the distribution of samples in Fig. 8a; for samples with low NO_3^-/Cl^- and Cl^-, concentration was influenced by soil nitrogen.

The mixing effects between different sources and mineralization-immobilization turnover (MIT) partially masked the real sources and initial isotope compositions. Hence, the high uncertainties in the apportionment gained by SIAR were inevitable and resulted from the broadly distributed proportion and the large standard deviation of potential sources. Despite the high uncertainties, SAM was the principal nitrate source for study area, with the lowest standard deviation among four potential sources. Therefore, reducing the output of SAM and the improvement of infrastructure in rural area are the key factors of nitrate contamination control in Nanyang Basin.

The high uncertainties were also a result of the collection of the isotope composition of main sources from the literature, which does not reflect the features in the study area; in addition, the sample numbers were too low. These limitations can be attributed to limited funds, although the results are still in agreement with those obtained via hydrochemical and stable isotope analyses.

Table 4 Summary of the $\delta^{15}N\text{-}NO_3^-$ and $\delta^{18}O\text{-}NO_3^-$ of different nitrate sources in the study area

Sources	$\delta^{15}N\text{-}NO_3^-$		$\delta^{18}O\text{-}NO_3^-$	
	Mean	SD	Mean	SD
Atmospheric deposition	3.2	2.4	44	9.1
Sewage and manure	16.3	5.7	7	2.7
Synthetic fertilizer	0.9	2	3.02[a]	0.55[a]
Soil Organic Nitrogen	5	1.5	3.02[a]	0.55[a]

[a] The $\delta^{18}O\text{-}NO_3^-$ of Sewage and manure and Soil Organic Nitrogen was calculated by Eq. (7), as the results of nitrification process

$\delta^{15}N\text{-}NO_3^-$ and $\delta^{18}O\text{-}NO_3^-$ of other sources were derived from literatures (Jin et al. 2018; Zhang et al., 2018; Li et al. 2019)
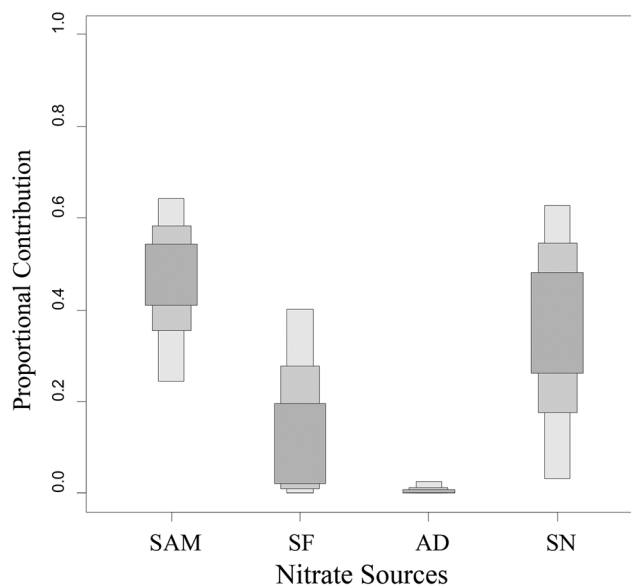

Fig. 10 Contributions of the four potential NO_3^- sources in the Nanyang Basin. Boxplots illustrate the 5, 25, 50, 75, and 95% credibility intervals of different sources for each sample

Uncertainty analysis

With the combined use of hydrochemical data, nitrate isotopes, and Bayesian mixing model, we thought our conclusion is reliable. Due to the following reasons, the uncertainties contained in our study were inevitable. The main reasons were as follows: (1) SIAR contains certain inherent uncertainties, and small variations of isotopic ranges for each potential nitrate sources may result in significant changes in sources apportionment; (2) the relatively limited number of nitrate isotopes measurements; (3) nitrogen cycle is a sophisticated biogeochemical process, and the study of nitrate pollution caused by the destruction of the nitrogen cycle balance requires a combination of multiple tracers.

Based on the above main reasons, the following points should be paid attention to in the future nitrate contamination studies: (1) accurately determining the isotopic ranges for potential nitrate sources. In a specific study area, the soil in uncultivated land, manure of breeding farms, wastewater for local sewage outfalls, and fertilizer from local market should be collected deliberately in order to reduce the uncertainties in the contribution calculated by SIAR; (2) if research funding is sufficient, samples considering different media (i.e., shallow aquifer, deep aquifer, and surface water), different land use types, and different time periods should be collected to determine the spatial and temporal variation of ions concentration and isotopes compositions; (3) due to nitrogen dynamic process is controlled by many environmental factors and multitracers should be combined use to study this issue. Such as groundwater travel time estimated by ^3H and chlorofluorocarbons (CFCs). Besides, measurements of $\delta^{15}N$ and $\delta^{18}O$ of NO_2^- and $\delta^{15}N\text{-}NH_4^+$ could further help identify the nitrogen

isotope fractionation process. Measurements of $\delta^{11}B$, $\delta^{87}Sr$, and coprostanol could help solve the problem of overlapping ranges of nitrate isotopes. (4) Analyzing the diversity and community composition of microorganisms and measure specific functional gene abundance can also help to determine the nitrogen transformation process, for this process is driven by microorganisms.

Conclusions

The shallow aquifer at the origin of the *South to North Water Diversion Project* in central China is subjected to considerable nitrate contamination. The average of nitrate concentration in this area was 102.95 ± 159.89 mg L^{-1}, indicating the strong mixing of potential sources to nitrate in our study area. With the aim to better identify sources and transformation processes of nitrate in groundwater, land use analysis, hydrochemistry, DIM ($\delta^{15}N$-NO$_3^-$ and $\delta^{18}O$-NO$_3^-$), and the Bayesian mixing model were used in combination. According to the molar ratio analysis and the significant correlation between the concentrations of nitrate and chloride, natural hydrochemical evolution was disturbed by anthropogenic activities.

Nitrification was the main process in subsoil and shallow aquifers, and the broadly distributed $\delta^{15}N$-NO$_3^-$ indicated that ammonium volatilization of SAM and the mixing effects between SAM and SF caused the enrichment of $\delta^{15}N$-NO$_3^-$. Denitrification was restricted by the oxidation environment in shallow aquifers, except for samples from some residential areas.

The Bayesian model (stable isotope analysis in R, SIAR) was used to apportion the contribution of potential sources, and sewage and manure were the dominant sources of nitrate, followed by soil nitrogen. The results of SIAR reflected the limitation of applying DIM in nitrate source determination, as the ranges of $\delta^{15}N$-NO$_3^-$ partially overlapped for SF and SN. As the result of recurrent mineralization-immobilization turnover during the leaching of irrigation and precipitation, the nitrate from SF may have contained $\delta^{15}N$-NO$_3^-$ from SN.

We could prove that despite the use of synthetic fertilizers, infrastructure and sewage disposal were the main factors contributing to nitrate contamination in the Nanyang Basin. Improved management strategies for untreated sewage are therefore critical to ensure the long-term water supply of the *South to North Water Diversion Project*.

Author's contribution Shengwei Cao: investigation, formal analysis, data curation, original draft

Yuhong Fei: supervision

Xia Tian: investigation, formal analysis

Xiangxiang Cui: investigation

Xueqiang Zhang: investigation

Ruoxi Yuan: investigation

Yasong Li*: supervision, funding acquisition, writing–review and editing

Declarations

Ethics approval and consent to participate This manuscript does not report on or involve the use of any animal or human data or tissue; therefore, it is not applicable for this part.

Consent for publication This manuscript does not contain any individual person's data in any form (including any individual details, images or videos); therefore, it is not applicable for this part.

Competing interests The authors declare no competing interests.

References

Aeschbach W, Gleeson T (2012) Regional strategies for the accelerating global problem of groundwater depletion. Nat Geosci 5:853–861

Arce MI, von Schiller D, Gómez R (2014) Variation in nitrate uptake and denitrification rates across a salinity gradient in Mediterranean semi-arid streams. Aquat Sci 76:295–311

Archana A, Thibodeau B, Geeraert N, Xu MN, Kao S-J, Baker DM (2018) Nitrogen sources and cycling revealed by dual isotopes of nitrate in a complex urbanized environment. Water Res 142:459–470

Atekwana EA, Geyer CJ (2018) Spatial and temporal variations in the geochemistry of shallow groundwater contaminated with nitrate at a residential site. Environ Sci Pollut Res 25:27155–27172

Bakeer S (2016) Effect of ammonium nitrate fertilizer and calcium chloride foliar spray on fruit cracking and sunburn of manfalouty pomegranate trees. Sci Hortic 209:300–308

Buccianti A, Nisi B, Martín-Fernández JA, Palarea-Albaladejo J (2014) Methods to investigate the geochemistry of groundwaters with values for nitrogen compounds below the detection limit. J Geochem Explor 141:78–88

Burkart MR, Kolpin DW (1993) Hydrologic and land-use factors associated with herbicides and nitrate in near-surface aquifers. J Environ Qual 22:646–656

Camacho-Cruz KA, Ortiz-Hernández MC, Sánchez A, Carrillo L, de Jesús Navarrete A (2020) Water quality in the eastern karst region

of the Yucatan Peninsula: nutrients and stable nitrogen isotopes in turtle grass, Thalassia testudinum. Environ Sci Pollut Res 27: 15967–15983

Chaudhuri Sriroop, Srinivasulu Ale, Delaune Paul, et al. (2012). Spatio-temporal variability of groundwater nitrate concentration in Texas: 1960 to 2010', 41: 1806-17.

Chen ZX, Yu L, Liu WG, Lam MHW, Liu G-J, Yin X-B (2014) Nitrogen and oxygen isotopic compositions of water-soluble nitrate in Taihu Lake water system, China: implication for nitrate sources and biogeochemical process. Environ Earth Sci 71:217–223

ChenMin-hua, X., Ling, M.-H., Zhou, Q., Zhang, Z.-C., Cheng, Q.-B., 2011. Numerical modeling the role of rubber dams on groundwater recharge and phreatic evaporation loss in riparian zones. Environmental Earth Sciences - ENVIRON EARTH SCI 65.

Clagnan, Elisa, Thornton Steven, Rolfe Stephen, et al. 2017. 'Influence of artificial drainage system design on the nitrogen attenuation potential of gley soils: evidence from hydrochemical and isotope studies under field-scale conditions', Journal of Environmental Management, 206.

Dan-Hassan, MA, Olasehinde PI, Amadi AN, et al. 2012. 'Spatial and temporal distribution of nitrate pollution in groundwater of Abuja, Nigeria', Spatial and Temporal Distribution of Nitrate Pollution in Groundwater of Abuja, Nigeria.

Deng X, Sun Y, Lei X et al (1996) Illite/smectite diagenesis in the NanXiang, Yitong, and North China Permian-Carboniferous Basins: application to petroleum exploration in China1. AAPG Bull 80:157–172

Deutsch B, Mewes M, Liskow I, Voss M (2006) Quantification of diffuse nitrate inputs into a small river system using stable isotopes of oxygen and nitrogen in nitrate. Org Geochem 37:1333–1342

Ding J, Xi B, Xu Q, Su J, Huo S, Liu H, Yu Y, Zhang Y (2015) Assessment of the sources and transformations of nitrogen in a plain river network region using a stable isotope approach. J Environ Sci 30:198–206

Du Y, Ma T, Deng Y et al (2017) Sources and fate of high levels of ammonium in surface water and shallow groundwater of the Jianghan Plain, Central China. Environ Sci Process Impacts 19: 161–172

Elisante, Eliapenda, and Muzuka Alfred. 2015. 'Occurrence of nitrate in Tanzanian groundwater aquifers: a review', Applied Water Science.

FAO. 2020. World Food and Agriculture - Statistical Yearbook 2020 (FAO: Rome, Italy).

Feth JH, Gibbs RJ (1971) Mechanisms controlling world water chemistry: evaporation-crystallization process. Science 172:870–872

Gautam S, Iqbal MZ (2010) Using stable isotopes of nitrogen to study its source and transformation in a heavily farmed watershed. Environ Earth Sci 60:11–20

Gibrilla A, Fianko JR, Ganyaglo S, Adomako D, Anornu G, Zakaria N (2020) Nitrate contamination and source apportionment in surface and groundwater in Ghana using dual isotopes (15N and 18O-NO3) and a Bayesian isotope mixing model. J Contam Hydrol 233: 103658

Granger, Julie, and Wankel Scott. 2016. 'Isotopic overprinting of nitrification on denitrification as a ubiquitous and unifying feature of environmental nitrogen cycling', Proceedings of the National Academy of Sciences, 113.

Guo Z, Yan C, Wang Z, Xu F, Yang F (2020) Quantitative identification of nitrate sources in a coastal peri-urban watershed using hydrogeochemical indicators and dual isotopes together with the statistical approaches. Chemosphere 243:125364

Hinshaw SE, Zhang T, John A. Harrison, et al. (2020) Excess N2 and denitrification in hyporheic porewaters and groundwaters of the San Joaquin River, California. Water Res 168:115161

Huizenga A, Bailey R, Gates T (2017) Stream-aquifer and in-stream processes affecting nitrogen along a major river and contributing tributary. J Contam Hydrol 199:24–35

Jin Z, Zheng Q, Zhu C, Wang Y, Cen J, Li F (2018) Contribution of nitrate sources in surface water in multiple land use areas by combining isotopes and a Bayesian isotope mixing model Applied Geochemistry:93

Ju XT, Kou CL, Zhang FS, Christie P (2006) Nitrogen balance and groundwater nitrate contamination: Comparison among three intensive cropping systems on the North China Plain. Environ Pollut 143: 117–125

Kaushal SS, Groffman PM, Band LE, Elliott EM, Shields CA, Kendall C (2011) Tracking nonpoint source nitrogen pollution in human-impacted watersheds. Environ Sci Technol 45:8225–8232

Kendall C, Ramón A, Cook PG et al (2000) Nitrate isotopes in groundwater systems. Environmental tracers in subsurface hydrology:261–298

Kendall Carol, Elliott M. Emily, Wankel D. Scott. 2007. Tracing anthropogenic inputs of nitrogen to ecosystems.' in K. Lajtha R. Michener (ed.), Stable isotopes in ecology and environmental science.

Kendall, Carol, Elliott Emily, and Wankel Scott. 2008. 'Tracing anthropogenic inputs of nitrogen to ecosystems.' in.

Kim K-H, Yun S-T, Choi B-Y, Chae G-T, Joo Y, Kim K, Kim H-S (2009) Hydrochemical and multivariate statistical interpretations of spatial controls of nitrate concentrations in a shallow alluvial aquifer around oxbow lakes (Osong area, central Korea). J Contam Hydrol 107:114–127

Kim KH, Yun ST, Mayer B, Lee J-H, Kim T-S, Kim H-K (2015) Quantification of nitrate sources in groundwater using hydrochemical and dual isotopic data combined with a Bayesian mixing model. Agric Ecosyst Environ 199:369–381

Kim H, Kaown D, Mayer B, Lee JY, Lee KK (2018) Combining pyrosequencing and isotopic approaches to assess denitrification in a hyporheic zone. Sci Total Environ 631-632:755–764

Knobeloch L, Salna B, Hogan A, Postle J, Anderson H (2000) Blue babies and nitrate-contaminated well water. Environ Health Perspect 108:675–678

Lasagna M, De Luca DA (2019) Evaluation of sources and fate of nitrates in the western Po plain groundwater (Italy) using nitrogen and boron isotopes. Environ Sci Pollut Res 26:2089–2104

Li Y, Yan W, Wang F, Lv S, Li Q, Yu Q (2019) Nitrogen pollution and sources in an aquatic system at an agricultural coastal area of Eastern China based on a dual-isotope approach. Environ Sci Pollut Res 26: 23807–23823

Liu M, Seyf-Laye ASM, Ibrahim T et al (2014) Tracking sources of groundwater nitrate contamination using nitrogen and oxygen stable isotopes at Beijing area, China. Environ Earth Sci 72:707–715

Lu L, Cheng H, Pu X, Liu X, Cheng Q (2015) Nitrate behaviors and source apportionment in an aquatic system from a watershed with intensive agricultural activities. Environ Sci Process Impacts 17: 131–144

Lunau M, Voss M, Erickson M et al (2012) Excess nitrate loads to coastal waters reduces nitrate removal efficiency: mechanism and implications for coastal eutrophication. Environ Microbiol 15

Ma Z, Yang Y, Lian X et al (2016) Identification of nitrate sources in groundwater using a stable isotope and 3DEEM in a landfill in Northeast China. Science of the Total Environment, s 563–564: 593–599

Ma P, Liu S, Yu Q, Li X, Han X (2019) Sources and transformations of anthropogenic nitrogen in the highly disturbed Huai River Basin, Eastern China. Environ Sci Pollut Res 26:11153–11169

Matiatos I (2016) Nitrate source identification in groundwater of multiple land-use areas by combining isotopes and multivariate statistical analysis: a case study of Asopos basin (Central Greece). Sci Total Environ 541:802–814

Mayer B, Bollwerk SM, Mansfeldt T, Hütter B, Veizer J (2001) The oxygen isotope composition of nitrate generated by nitrification in acid forest floors. Geochim Cosmochim Acta 65:2743–2756

Meghdadi A, Javar N (2018a) Evaluation of nitrate sources and the percent contribution of bacterial denitrification in hyporheic zone using isotope fractionation technique and multi-linear regression analysis. J Environ Manag 222:54–65

Meghdadi A, Javar N (2018b) Quantification of spatial and seasonal variations in the proportional contribution of nitrate sources using a multi-isotope approach and Bayesian isotope mixing model. Environ Pollut 235:207–222

Menció A, Mas-Pla J, Otero N, Regàs O, Boy-Roura M, Puig R, Bach J, Domènech C, Zamorano M, Brusi D, Folch A (2016) Nitrate pollution of groundwater; all right…, but nothing else? Sci Total Environ 539:241–251

Mengis M, Walther U, Bernasconi S et al (2001) Limitations of using ?? 18 O for the source identification of nitrate in agricultural soils. Environ Sci Technol 35:1840–1844

Meybeck M (1982) Carbon, nitrogen, and phosphorus transport by world rivers. Am J Sci 282:401–450

Minet E, Coxon C, Goodhue R et al (2012) Evaluating the utility of N-15 and O-18 isotope abundance analyses to identify nitrate sources: a soil zone study. Water Res 46:3723–3736

Minet, EP, Goodhue R, Meier-Augenstein W, et al. 2017. 'Combining stable isotopes with contamination indicators: a method for improved investigation of nitrate sources and dynamics in aquifers with mixed nitrogen inputs', 124: 85,

Murgulet D, Tick GR (2013) Understanding the sources and fate of nitrate in a highly developed aquifer system. J Contam Hydrol 155: 69–81

Nanyang Municipal Government. (2019). *Nanyang Statistical Yearbook (in Chinese)* (China Statistics Yearbook: Nanyang, China).

Oberhelman, Andrew, and Peterson Eric. 2020. 'Chloride source delineation in an urban-agricultural watershed: deicing agents versus agricultural contributions', Hydrological Processes.

Parnell AC, Inger R, Bearhop S, Jackson AL (2010) Source partitioning using stable isotopes: coping with too much variation. PLoS One 5: e9672

Pasten-Zapata E, Ledesma R, Harter T, Ramirez A, Mahlknecht J (2014) Assessment of sources and fate of nitrate in shallow groundwater of an agricultural area by using a multi-tracer approach. Sci Total Environ 470-471:855–864

Piske J, Peterson E (2020) The role of corn and soybean cultivation on nitrate export from Midwestern US agricultural watersheds. Environ Earth Sci 79

Rahmati O, Melesse A (2016) Application of Dempster–Shafer theory, spatial analysis and remote sensing for groundwater potentiality and nitrate pollution analysis in the semi-arid region of Khuzestan, Iran. Sci Total Environ 568:1110–1123

Roadcap, George, Keith Hackley, and Hue-Hwa Hwang. 2002. 'Application of nitrogen and oxygen isotopes to identify sources of nitrate'.

Roy S, Gaillardet J, Allègre CJ (1999) Geochemistry of dissolved and suspended loads of the Seine River, France: anthropogenic impact, carbonate and silicate weathering. Geochim Cosmochim Acta 63: 1277–1292

Sheikhy NT, Aris AZ, Sefie A et al (2017) Detecting and predicting the impact of land use changes on groundwater quality, a case study in Northern Kelantan, Malaysia. Sci Total Environ 599-600:844–853

Shi X, Dong W, Li M, Zhang Y (2012) Evaluation of groundwater renewability in the Henan Plains, China. Geochem J 46:107–115

Sigman D, Casciotti K, Andreani M et al (2001) A bacterial method for the nitrogen isotopic analysis of nitrate in seawater and freshwater. Anal Chem 73:4145–4153

Soto DX, Koehler G, Leonard I. Wassenaar, et al. (2019) Spatio-temporal variation of nitrate sources to Lake Winnipeg using N and O isotope (δ15N, δ18O) analyses. Sci Total Environ 647:486–493

Spalding R, Hirsh AJ, Exner ME et al (2018a) 'Applicability of the dual isotopes δ15N and δ18O to identify nitrate in groundwater beneath irrigated cropland. J Contam Hydrol:220

Spalding R, Hirsh A, Exner M et al (2018b) 'Integrated deep soil n and groundwater isotope investigation of n sources captured by municipal wells. Groundwater Monitoring & Remediation:39

Su X, Wang H, Zhang Y (2013) Health risk assessment of nitrate contamination in groundwater: a case study of an agricultural area in northeast China. Water Resour Manag 27:3025–3034

Taufiq A, Effendi AJ, Iskandar I, Hosono T, Hutasoit LM (2019) Controlling factors and driving mechanisms of nitrate contamination in groundwater system of Bandung Basin, Indonesia, deduced by combined use of stable isotope ratios, CFC age dating, and socio-economic parameters. Water Res 148:292–305

Torres-Martínez JA, Mora A, Mahlknecht J, Daesslé LW, Cervantes-Avilés PA, Ledesma-Ruiz R (2021) Estimation of nitrate pollution sources and transformations in groundwater of an intensive livestock-agricultural area (Comarca Lagunera), combining major ions, stable isotopes and MixSIAR model. Environ Pollut 269: 115445

Wang S, Tang C, Song X, Yuan R, Wang Q, Zhang Y (2013) Using major ions and δ15N-NO3- to identify nitrate sources and fate in an alluvial aquifer of the Baiyangdian lake watershed, North China Plain. Environ Sci Process Impacts 15:1430–1443

Wang Z-h, Miao Y-f, Li S-x (2015) Effect of ammonium and nitrate nitrogen fertilizers on wheat yield in relation to accumulated nitrate at different depths of soil in drylands of China. Field Crop Res 183: 211–224

Wang S, Zheng W, Currell M et al (2017) Relationship between land-use and sources and fate of nitrate in groundwater in a typical recharge area of the North China. Plain 609:607–620

Wick K, Heumesser C, Schmid E (2011) Groundwater nitrate contamination: factors and indicators. J Environ Manag 111:178–186

Widory D, Petelet-Giraud E, Négrel P, Ladouche B (2005) Tracking the sources of nitrate in groundwater using coupled nitrogen and boron isotopes: a synthesis. Environ Sci Technol 39:539–548

World Health Organization. 2003. "Nitrate and nitrite in drinking-water: background document for development of WHO guidelines for drinking-water quality." In. Geneva: World Health Organization.

Wu, Fengchang, Feng Weiying, Guo Wenjing, et al. 2018. 'Using dual isotopes and a Bayesian isotope mixing model to evaluate sources of nitrate of Tai Lake, China', Environmental Science and Pollution Research, 25.

Xue D, Botte J, De Baets B et al (2009) Present limitations and future prospects of stable isotope methods for nitrate source identification in surface and groundwater. Water Res 43:1159–1170

Xue D, De Baets B, Van Cleemput O et al (2012) Use of a Bayesian isotope mixing model to estimate proportional contributions of multiple nitrate sources in surface water. Environ Pollut 161:43–49

Yang L, Han J, Xue J et al (2013) Nitrate source apportionment in a subtropical watershed using Bayesian model. Sci Total Environ 463:340–347

Zhang Q, Wang H, Wang L (2018a) Tracing nitrate pollution sources and transformations in the over-exploited groundwater region of north China using stable isotopes. J Contam Hydrol 218:1–9

Zhang Y, Shi P, Li F, Wei A, Song J, Ma J (2018b) Quantification of nitrate sources and fates in rivers in an irrigated agricultural area using environmental isotopes and a Bayesian isotope mixing model. Chemosphere:208